Journal of Sound and Vibration (2000) **233**(5), 745–759
doi:10.1006 jsvi.1998.2077, available online at http://www.idealibrary.com on IDEAL

MULTIPLE REFERENCE FEEDFORWARD ACTIVE NOISE CONTROL PART I: ANALYSIS AND SIMULATION OF BEHAVIOR

Y. Tu and C. R. Fuller

Vibration and Acoustic Laboratories, Mechanical Engineering Department, Virginia Polytechnic Institute and State University, Blacksburg, VA 24061-0238, *U.S.A.*

(*Received* 6 *June* 1997, *and in final form* 13 *November* 1998)

In this work, two forms of frequency domain optimum solutions for multiple reference active noise control (MRANC) in a feedforward arrangement are given in terms of signal spectra and system frequency response functions (FRF). It is particularly noted that the optimum solutions are uncoupled if the reference signals are uncorrelated or the noise sources are directly available as reference signals. Other than the traditional control configuration which feed each reference signal into a different filter, another control configuration which combines multiple reference signals into a single input is also investigated. Although this configuration generally delivers a compromised control effect, the payoff is a simplified control structure and significant computational savings. In addition, under some circumstances, the desired performance which is comparable to other complex configurations can be achieved. Simulations based on sound transmission through a vibrating plate have been conducted and the results presented are consistent with the theoretical analysis.

© 2000 Academic Press

1. INTRODUCTION

Over the last two decades, active noise control (ANC) has been demonstrated as an effective approach for low frequency noise reduction. The principle of ANC is based on the superposition of the two acoustical waves from the primary and secondary sources. When the two waves are out of phase and of the same amplitude, the superposition results in complete cancellation of the two waves and therefore generates a silent zone. ANC provides an ideal complement to the conventional passive noise control approach, which generally works efficiently at higher frequencies.

The application of ANC has been extended from single noise source one-dimensional acoustical fields, e.g., a low frequency field in an air duct, to complex multiple noise sources in three-dimensional acoustical fields, e.g., a sound field in an aircraft cabin. The extension to three-dimensional acoustical fields requires a number of secondary sources to minimize the mean square signals from a number of error sensors, so that the primary acoustical field can be spatially matched [1]. The extension to a multiple noise source environment usually requires more than one reference sensor to generate a complete set of reference signals [2].

An important issue for multiple reference active noise control (MRANC) is the selection of the number and the positions of reference sensors. The principle for reference sensor selection is based on using a minimum number of reference sensors to

0022–460X/00/250745 + 15 $35.00/0 © 1999 Academic Press

achieve maximum multiple coherence between the reference signals and the primary noise signals. The number of reference sensors should be as small as possible in order to simplify control structure and save computational cost, while the multiple coherence function should be as close to unity as possible in order to achieve maximum noise reduction [2]. Generally speaking, the reference sensors should be able to detect all the independent noise sources, which usually implies more reference sensors than independent noise sources [3]. A number of frequency domain approaches have been applied to identify noise sources based on coherence techniques [4, 5] and Principal Component Analysis [6]. The applicability of coherence techniques is determined by the correlation among reference signals. Principle Component Analysis is effective in determining the dominant noise sources and does not depend on the correlation among reference signals. However, the exact locations of reference sensors required to detect those noise sources remain unknown. Recently, attention has been paid on the convergence rate as well as the number of controller coefficients for reference sensor selection [7].

The previous studies of multiple reference active noise control are mainly focused on noise source identification and reference sensor selection. An important issue remains untouched. When MRANC is designed to achieve noise reduction at a number of locations or globally, the control structure becomes very complicated and the amount of computations may exceed the computational limit of many digital signal processors (DSP). It is therefore of much significance to study the possibility of simplifying the MRANC control structure, while maintaining the desired noise reduction. In addition, the coupling effect between noise sources and reference sensors has not been directly investigated.

2. FREQUENCY DOMAIN ANALYSIS

Figure 1 shows a typical MRANC system, in which there are M noise sources, K reference sensors, one secondary source and one error sensor. Each reference signal is

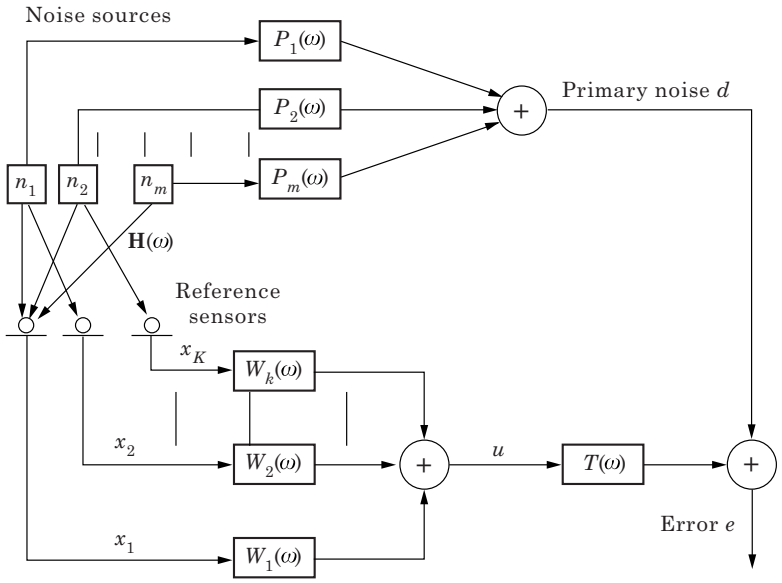

Figure 1. Multiple reference multiple input (MRMI) system.

fed into a different filter and the output of each filter is summed together to drive a single secondary source. This multiple reference multiple input (MRMI) configuration for processing reference signals attempts to control the primary noise from multiple primary paths with the secondary noise from multiple filters, thus it enjoys the applicability in general situations and has been adopted in most previous studies [2, 8]. Since the number of the secondary sources and error sensors is chosen to be unity to simplify the analysis, spatial noise reduction effect is not a concern. The signal at the error sensor is the superposition of the primary noise and the secondary noise and is given by

$$e(\omega) = d(\omega) + T(\omega)\mathbf{x}^T(\omega)\mathbf{W}(\omega), \tag{1}$$

where $d(\omega)$ is the primary noise, $T(\omega)$ is the frequency response function (FRF) between the secondary source and the error sensor, $\mathbf{x}(\omega)$ is the reference signal vector, and $\mathbf{W}(\omega)$ is the controller FRF vector, that is

$$\mathbf{x}(\omega) = \{x_1(\omega)x_2(\omega)\cdots x_k(\omega)\}^T, \quad \mathbf{W}(\omega) = \{W_1(\omega)W_2(\omega)\cdots W_k(\omega)\}^T. \tag{2, 3}$$

The objective of ANC is to minimize the error signal, thus the cost function is defined as

$$\xi(\omega) = \mathrm{E}(e^*(\omega)e(\omega)), \tag{4}$$

where the asterisk * denotes the complex conjugate. Substituting equation (1) into equation (4) and taking the complex derivative with respect to the controller vector [9], the gradient of the cost function is obtained as

$$\nabla = \mathrm{E}(\hat{\mathbf{x}}^*(\omega)\hat{\mathbf{x}}^T)\mathbf{W}(\omega) + \mathrm{E}(d(\omega)\hat{\mathbf{x}}^*(\omega)), \tag{5}$$

where

$$\hat{\mathbf{x}}(\omega) = \mathbf{x}(\omega)T(\omega). \tag{6}$$

The optimum controller vector can be obtained by setting the gradient to zero, thus

$$\mathbf{W}_{\mathrm{opt}}(\omega) = -\mathbf{R}^{-1}(\omega)\mathbf{P}(\omega), \tag{7}$$

where $\mathbf{R}(\omega)$ is a matrix, whose diagonal terms are the auto-spectra of the reference signals and off-diagonal terms are the cross-spectra of the reference signals, $\mathbf{P}(\omega)$ is a vector representing the cross-spectra between the reference signals and the primary noise, i.e.,

$$\mathbf{R}(\omega) = \begin{pmatrix} S_{\hat{x}_1\hat{x}_1}(\omega) & S_{\hat{x}_1\hat{x}_2}(\omega) & \cdots & S_{\hat{x}_1\hat{x}_k}(\omega) \\ S_{\hat{x}_2\hat{x}_1}(\omega) & S_{\hat{x}_2\hat{x}_2}(\omega) & \cdots & S_{\hat{x}_2\hat{x}_k}(\omega) \\ \vdots & \vdots & \vdots & \vdots \\ S_{\hat{x}_k\hat{x}_1}(\omega) & S_{\hat{x}_1\hat{x}_2}(\omega) & \cdots & S_{\hat{x}_k\hat{x}_k}(\omega) \end{pmatrix}, \quad \mathbf{P}(\omega) = \begin{pmatrix} S_{\hat{x}_1 d}(\omega) \\ S_{\hat{x}_2 d}(\omega) \\ \vdots \\ S_{\hat{x}_k d}(\omega) \end{pmatrix}. \tag{8, 9}$$

It is interesting to note that if the reference signals are uncorrelated, their cross-spectra would be zero. It follows that all the off-diagonal terms inside the matrix $\mathbf{R}(\omega)$ are zero. Thus, equation (7) can be rewritten as

$$W_{i,opt}(\omega) = \frac{S_{\hat{x}_i d}(\omega)}{S_{\hat{x}_i\hat{x}_i}(\omega)}, \quad i = 1, 2, 3 \ldots k. \tag{10}$$

The above equation indicates that the optimum solutions of all the filters are independent, and each filter operates without any interference from other filters. In other

words, the filters are uncoupled if the reference signals are uncorrelated. The optimum controller vector can be derived in terms of system FRF's. The primary noise at the error sensors is formed by M noise sources passing through M primary paths and is given by

$$d(\omega) = \mathbf{n}^T(\omega)\mathbf{P}(\omega), \tag{11}$$

where $\mathbf{n}(\omega)$ and $\mathbf{P}(\omega)$ are noise source vector and primary FRF vector, respectively, and can be expressed as

$$\mathbf{n}(\omega) = \{n_1(\omega)n_2(\omega)\cdots n_m(\omega)\}^T, \quad \mathbf{P}(\omega) = \{P_1(\omega)P_2(\omega)\cdots P_m(\omega)\}^T. \tag{12, 13}$$

The M noise sources are assumed to be uncorrelated with each other, which implies that any one of the noise sources can not be obtained by linear transformations of other noise sources. It should be noted that if the M uncorrelated noise sources have Gaussian distribution, they are also independent [10]. The noise sources and the reference signals are related by

$$\mathbf{x}(\omega) = \mathbf{H}(\omega)\mathbf{n}(\omega), \tag{14}$$

where $\mathbf{H}(\omega)$ is the source coupling matrix, whose element $H_{ij}(\omega)$ represents the FRF between the ith noise source and the jth reference sensor, and can be written as

$$\mathbf{H}(\omega) = \begin{pmatrix} H_{11}(\omega) & H_{21}(\omega) & \cdots & H_{m1}(\omega) \\ H_{21}(\omega) & H_{22}(\omega) & \cdots & H_{m2}(\omega) \\ \vdots & \vdots & \vdots & \vdots \\ H_{k1}(\omega) & H_{k2}(\omega) & \cdots & H_{mk}(\omega) \end{pmatrix}. \tag{15}$$

Substituting equations (6), (11), and (14) into equation (5) and moving all the FRFs to the outside of the expectation operator, the gradient of the cost function is obtained as

$$\nabla = T^*(\omega)\mathbf{H}^*(\omega)\mathrm{E}(\mathbf{n}^*(\omega)\mathbf{n}^T(\omega)\lfloor\mathbf{H}^T(\omega)T(\omega)\mathbf{W}(\omega) + \mathbf{P}(\omega)\rfloor. \tag{16}$$

Another form of optimum controller vector can be obtained by setting the gradient to zero, i.e.,

$$\mathbf{W}_{opt}(\omega) = -\mathbf{H}^+(\omega)\frac{\mathbf{P}(\omega)}{T(\omega)}, \tag{17}$$

where $\mathbf{H}^+(\omega)$ is the pseudo-inverse [11] of $\mathbf{H}^{\mathrm{T}}(\omega)$. The optimum controller vector is expressed in terms of FRFs of the primary path $\mathbf{P}(\omega)$, the error path $T(\omega)$ and the source coupling path $\mathbf{H}(\omega)$. This solution is intuitively clear: the error signal comes from the noise sources through both the primary path and the secondary path, the controller in the secondary path adjusts its FRF so that the two paths have the same magnitude response and 180° phase difference. Thus, noise cancellation is achieved.

If $\mathbf{H}(\omega)$ is an identity matrix, which implies that the number of reference sensors is the same as the number of noise sources, and each noise source is available as reference signal, equation (17) reduces to

$$W_{i,opt}(\omega) = -\frac{P_i(\omega)}{T(\omega)}. \tag{18}$$

Again, equation (18) indicates that the optimum solutions of all the control filters are independent. In fact, each optimum solution is determined only by the corresponding primary path and the error path.

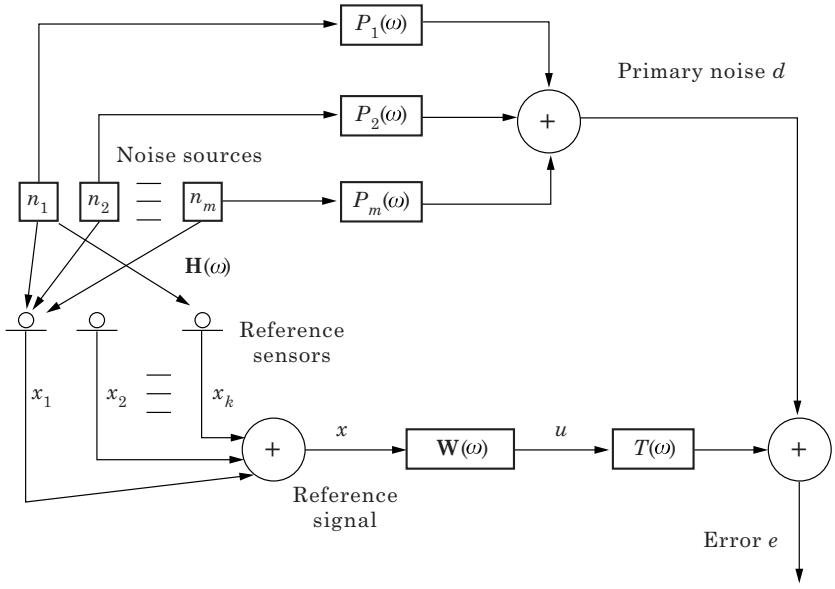

Figure 2. Multiple reference single input (MRSI) system.

An alternative MRANC system combines all the reference signals into a single input (MRSI), as shown in Figure 2. This configuration generally delivers compromised noise reduction effect. However, under some special circumstances, the desired noise reduction effect along with a large number of computational savings can be obtained. The coherence function between the primary noise and the reference signal is defined as

$$\gamma(\omega) = \frac{S_{xd}(\omega)S_{dx}(\omega)}{S_{xx}(\omega)S_{dd}(\omega)}. \tag{19}$$

The primary noise and the reference signal can be written as

$$d(\omega) = n_1(\omega)P_1(\omega) + n_2(\omega)P_2(\omega) + \cdots + n_M(\omega)P_M(\omega), \tag{20}$$

$$x(\omega) = n_1(\omega)H_1(\omega) + n_2(\omega)H_2(\omega) + \cdots + n_M(\omega)H_M(\omega), \tag{21}$$

where $H_j(\omega)$ is the summation of all the FRFs from the ith noise sources to all the reference sensor and is given by

$$H_i(\omega) = \sum_{j=1}^{K} H_{ij}(\omega). \tag{22}$$

Since the noise sources are assumed to be uncorrelated, their cross-spectra are zero, it follows that

$$S_{xx} = S_{n_1n_1}|H_1|^2 + S_{n_2n_2}|H_2|^2 + \cdots + S_{n_kn_k}|H_k|^2, \tag{23}$$

$$S_{dd} = S_{n_1n_1}|P_1|^2 + S_{n_2n_2}|P_2|^2 + \cdots + S_{n_kn_k}|P_k|^2, \tag{24}$$

$$S_{xd} = S_{n_1n_1}H_1^*P_1 + S_{n_2n_2}H_2^*P_2 + \cdots + S_{n_kn_k}H_k^*P_k, \tag{25}$$

$$S_{dx} = S_{n_1n_1}H_1P_1^* + S_{n_2n_2}H_2P_2^* + \cdots + S_{n_kn_k}H_kP_k^*. \tag{26}$$

In the above equations, the frequency symbol ω is skipped for simplicity. Subtracting the

numerator from the denominator of the coherence function defined in equation (19) results in

$$\begin{aligned} & S_{xx}S_{dd} - S_{xd}S_{dx} \\ & = \sum_{i,j-1,i\neq j}^{k} (S_{n_in_i}S_{n_jn_j}(|H_i|^2|P_j|^2 + |H_j|^2|P_i|^2 - H_iH_j^*P_i^*P_j - H_i^*H_jP_iP_j^*)) \\ & = \sum_{i,j=1,i\neq j}^{k} (S_{n_in_i}S_{n_jn_j}(|H_iP_j - H_jP_i|^2)). \end{aligned} \tag{27}$$

Since the auto-spectrum is non-negative, the above expression is also non-negative, which implies that the coherence function is less than or equal to unity, i.e.,

$$\gamma(\omega) \leqslant 1. \tag{28}$$

This result indicates that perfect noise cancellation may not be achievable with the MRSI configuration. It should be noted that since there are no unaccounted input signals, output signals, or non-linear components in the system, if the system is configured properly, unity coherence function is expected. Thus, the coherence inadequacy is caused by the defect of the MRSI configuration. It is also important to note that the MRSI configuration is defective even when the reference signals are uncorrelated. This conclusion can be seen by assuming that each noise source is available as a reference signal, accordingly, every noise coupling term H_i in equation (27) drops out and equation (28) still holds. As a conclusion, compromised noise reduction is anticipated as a result of the defective MRSI control structure.

However, attention should be given to two special circumstances: (1) $S_{n_in_i}S_{n_jn_j} = 0$, for $i \neq j$, which indicates that each reference signal occupies a different frequency range; (2) $|H_iP_j - H_jP_i| = 0$, for $i \neq j$, which may result from the case when each noise source is available as a reference signal, and all the FRFs of the primary paths are equal. Under the above two circumstances, equation (26) is equal to zero, which implies unity coherence function throughout the frequency range. Thus, when either one of the above two conditions is met, the performance of a MRSI configuration is expected to be equivalent to that of a MRMI configuration. For example, when several engines run at different speeds, each engine can be considered as a source radiating only tonal noise, since the base tone frequency is different, a MRSI configuration can be used to obtain desired noise reduction. This falls into the first circumstance. If the noise sources are adjacently located and available as reference signals without coupling, and the error sensors are far away from the noise sources, all the primary paths are expected to be comparable. As a result, the desired noise reduction effect can be achieved with a MRSI configuration. This falls into the second circumstance. The choice of a MRSI configuration significantly simplifies a MRANC system as compared to a MRMI configuration.

3. SIMULATION SET-UP AND SYSTEM MODELLING

In the previous section, the frequency domain optimum solution of a typical MRANC system is derived followed by the performance comparison of two distinct configurations using coherence analysis. In order to verify the theoretical results, computer simulations are carried out with the transfer functions based on an actual MRANC system discussed below.

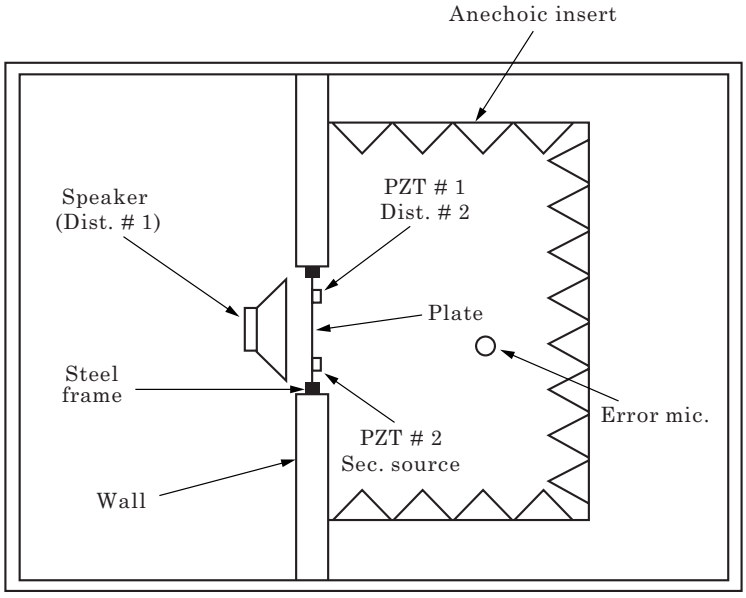

Figure 3. Experimental set-up.

As shown in Figure 3, there are two disturbance sources, one secondary source and one error microphone for the plate system. With the dimension of 0·381 m long and 0·305 m wide, the plate is mounted in a heavy steel frame, which produces negligible rotation and displacement of the boundary, approximating clamped boundary conditions. The steel frame is further mounted in a rigid wall with one side facing toward a reverberation chamber and the other side toward an anechoic chamber. The plate is excited by two distinctive noise sources; one is the acoustical disturbance from a large speaker, while the other is the structural disturbance from a piezoelectric ceramic transducer (PZT #1) mounted on the plate. The secondary control source acting on the plate is another piezoelectric actuator (PZT #2). The positions of both of the PZTs are selected such that any plate mode of order (4,4) or less can be excited, as shown in Table 1. The error sensor is a microphone located in the direction approximately perpendicular to the center of the plate, but slightly off the center such that the even modes of the plate have relatively small noise contribution, but are still observable and controllable. The goal of the control is to minimize the total radiated sound at the error microphone. The two particular noise sources are chosen in an effort to simulate what happens in an aircraft cabin, which may generate interior noise due to directly applied structural forces as well as acoustical pressure fluctuations acting on it from the exterior.

The system shown in Figure 3 has two primary paths (from the speaker through the plate to the error microphone and from the PZT #1 to the error microphone) and one error path (from the PZT #2 to the error microphone). The FRFs of the two primary paths and the error path were modelled with FIR filters. In order to obtain the FIR models of the system, the FRFs were measured with a B&K 2032 digital signal analyzer,

TABLE 1

Excited modes and measured natural frequencies of the clamped plate

Mode	(1,1)	(2,1)	(1,2)	(2,2)	(3,1)
Frequency (Hz)	115	201	265	342	350

and 801 frequency response data samples equally spaced between 0 and 400 Hz were obtained. These frequency response data were fitted with FIR filters using the least square method [12]. The frequency range is constrained to be below 400 Hz. Within the chosen frequency range, a maximum of five structural modes can be excited.

The number of coefficients in each FIR filter was chosen to be 128 such that both the phase and magnitude of the FRF can be well matched at the frequency range where large noise cancellation is desired. The match at other frequency ranges (e.g., below 40 Hz) is not very important, since the noise cancellation at those frequency ranges is unobtainable due to the dynamic limitations of the PZT actuators. The sampling frequency is chosen to be 800 Hz, which is exactly the Nyquist frequency for the system. The measured frequency response functions and their corresponding FIR models are shown in Figures 4–6. The speaker excitation acting normal to the plate has the dominant frequency response at the (1,1) mode, as shown in Figure 4. The two PZT

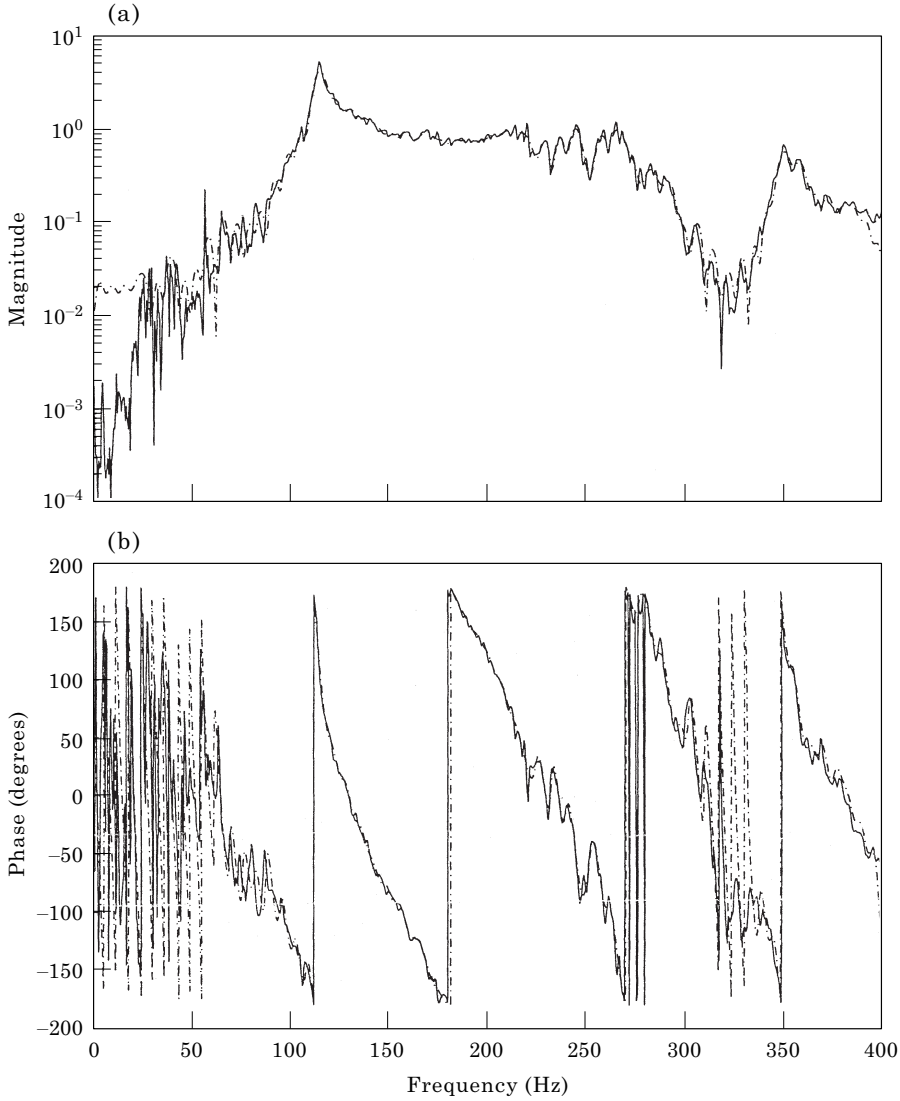

Figure 4. Frequency response function ((a) magnitude, (b) phase) and its FIR model for the primary path no. 1: —, measured transfer function; –·–·–, FIR model.

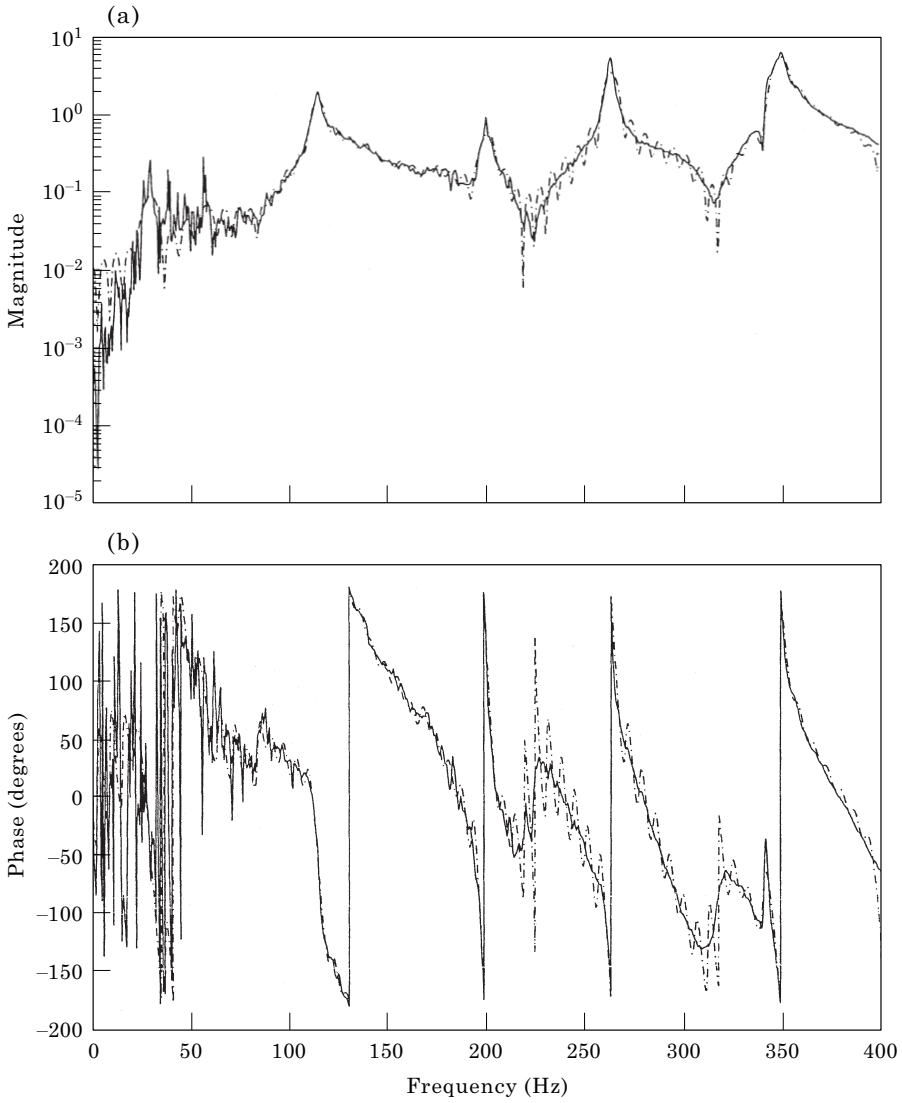

Figure 5. Frequency response function ((a) magnitude, (b) phase) and its FIR model for the primary path no.2: —, measured transfer function; –·–·–, FIR model.

excitations generate similar frequency response due to their physical locations at the plate.

4. SIMULATION RESULTS

In the first simulation, the performance difference of the two configurations (MRSI and MRMI) is examined with two independent random signal generators as the noise sources. For the MRMI configuration, the two reference signals are obtained directly from the two random signal generators. For the MRSI configuration, the reference signal is the summation of the signals from the two random signal generators. The optimum filter weight vectors for both configurations are calculated based on the norm equation, which will be derived in detail in part II of this paper. Here the result is given

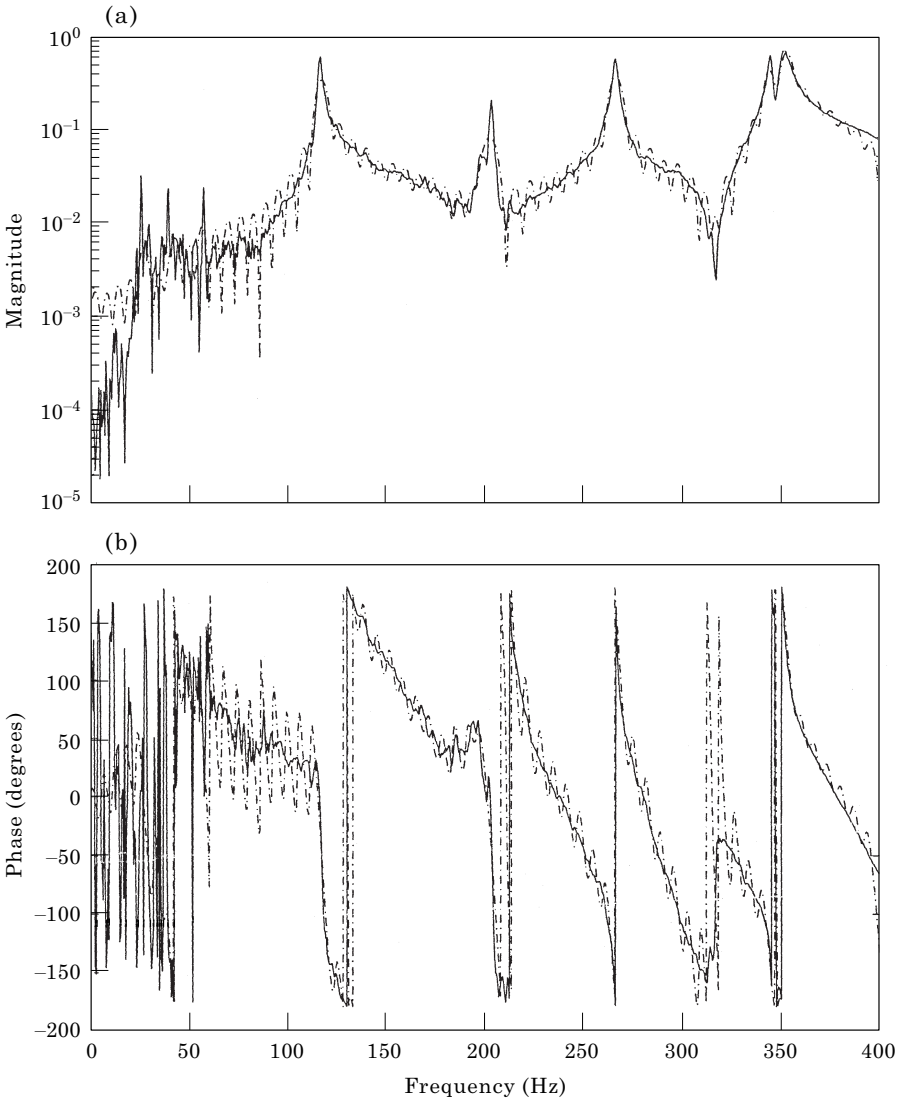

Figure 6. Frequency response function ((a) magnitude, (b) phase) and its FIR model for the error path: —, measured transfer function; –·–·–, FIR model.

as

$$\mathbf{R}\mathbf{W}_{opt} = -\mathbf{P}, \tag{29}$$

where

$$\mathbf{R} = E\begin{pmatrix} \hat{\mathbf{x}}_1(k)\hat{\mathbf{x}}_1^T(k) & \hat{\mathbf{x}}_1(k)\hat{\mathbf{x}}_2^T(k) & \cdots & \hat{\mathbf{x}}_1(k)\hat{\mathbf{x}}_k^T(k) \\ \hat{\mathbf{x}}_2(k)\hat{\mathbf{x}}_1^T(k) & \hat{\mathbf{x}}_2(k)\hat{\mathbf{x}}_2^T(k) & \cdots & \hat{\mathbf{x}}_2(k)\hat{\mathbf{x}}_k^T(k) \\ \vdots & \vdots & \vdots & \vdots \\ \hat{\mathbf{x}}_k(k)\hat{\mathbf{x}}_1^T(k) & \hat{\mathbf{x}}_k(k)\hat{\mathbf{x}}_2^T(k) & \cdots & \hat{\mathbf{x}}_k(k)\hat{\mathbf{x}}_k^T(k) \end{pmatrix}, \quad \mathbf{P} = E\begin{pmatrix} \hat{\mathbf{x}}_1(k)d(k) \\ \hat{\mathbf{x}}_2(k)d(k) \\ \vdots \\ \hat{\mathbf{x}}_k(k)d(k) \end{pmatrix}. \tag{30, 31}$$

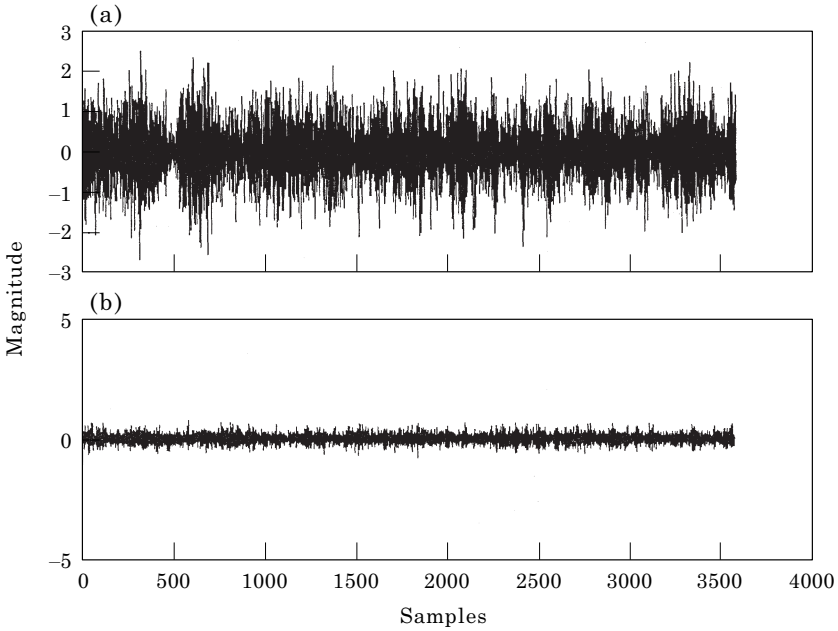

Figure 7. Error signal after control in a typical case: (a) MRSI (b) MRMI control.

The expected values inside the matrix **R** and the vector **P** were approximated using the average of 4096 samples. The residual noise after control is obtained by substituting the optimum weight vectors into controller filters.

The error signal after control (residual noise) in the time domain is shown in Figure 7, which indicates that the error signal for MRMI is much smaller than that for MRSI. In other words, MRMI achieves much better noise reduction than MRSI. Although perfect noise cancellation with MRMI can be achieved theoretically since the system is casual, completely coherent and without any additional noise, the error signal does not reach zero. This is due to the finite filter length effect since each controller filter for MRMI has only 128 coefficients. A comparison of the power spectral density is shown in Figure 8, which clearly indicates that the performance of MRMI is much better than that of MRSI. In fact, 10 dB overall noise reduction for MRMI is achieved, while only about 3 dB overall noise reduction is achieved for MRSI. It should be noted that the maximum noise reduction occurs in the vicinity of the resonance frequencies, while at the off-resonance frequencies, only a small amount of noise attenuation is achieved. It is also evident that the maximum noise reduction occurs at the frequency ranges of 110–200 and 340–400 Hz. This result is expected since the odd modes of the plates, i.e., (1,1), and (1,3) modes, matching the two frequency ranges, have dominant noise contribution at the error sensor due to the microphone location. In this simulation, the controller filter in MRSI has 128 coefficients and each of the two filters in MRMI has 128 coefficients; further investigation shows that increasing the number of coefficients in MRSI does not improve the noise reduction effect significantly.

Since both noise sources in the preceding simulation have the same frequency range between 0 and 400 Hz, the poor performance of MRSI is expected. However, if the two noise sources have a non-overlapped frequency range, MRSI is expected to have comparable performance with MRMI. In this simulation, the first noise source is provided by a random signal generator passing through a low-pass filter with a cut-off frequency at 160 Hz, and the second noise source is provided by another random signal

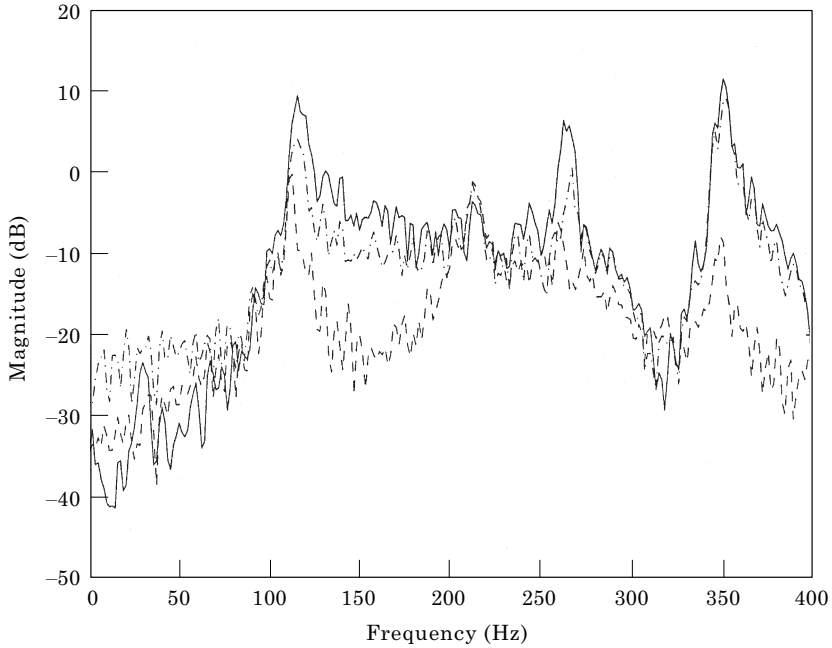

Figure 8. Spectrum of error signal in a typical case: —, before control; –·–·–, with MRSI control; – – –, with MRMI control.

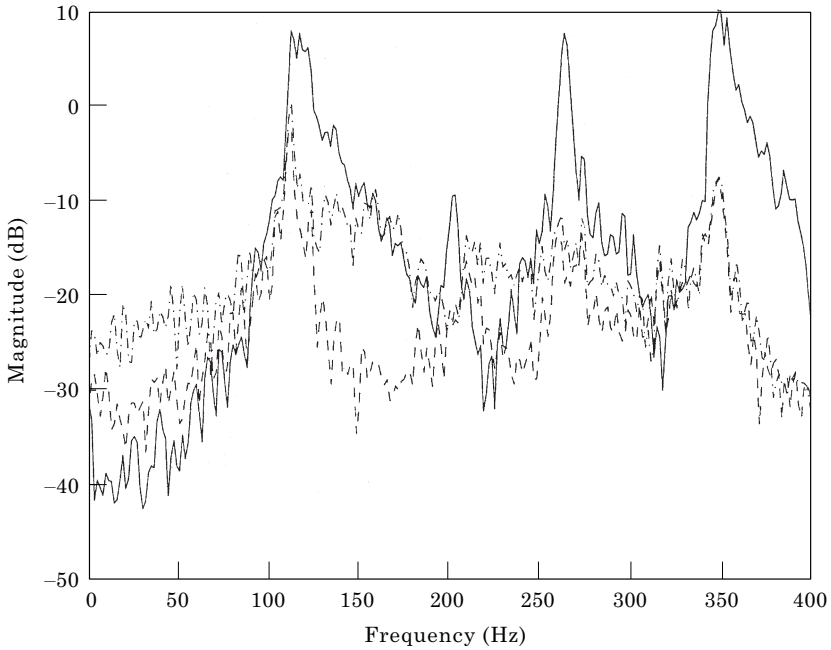

Figure 9. Spectrum of error signal when each noise source occupies different frequency bands: —, before control; –·–·–, with MRSI control; – – –, with MRMI control.

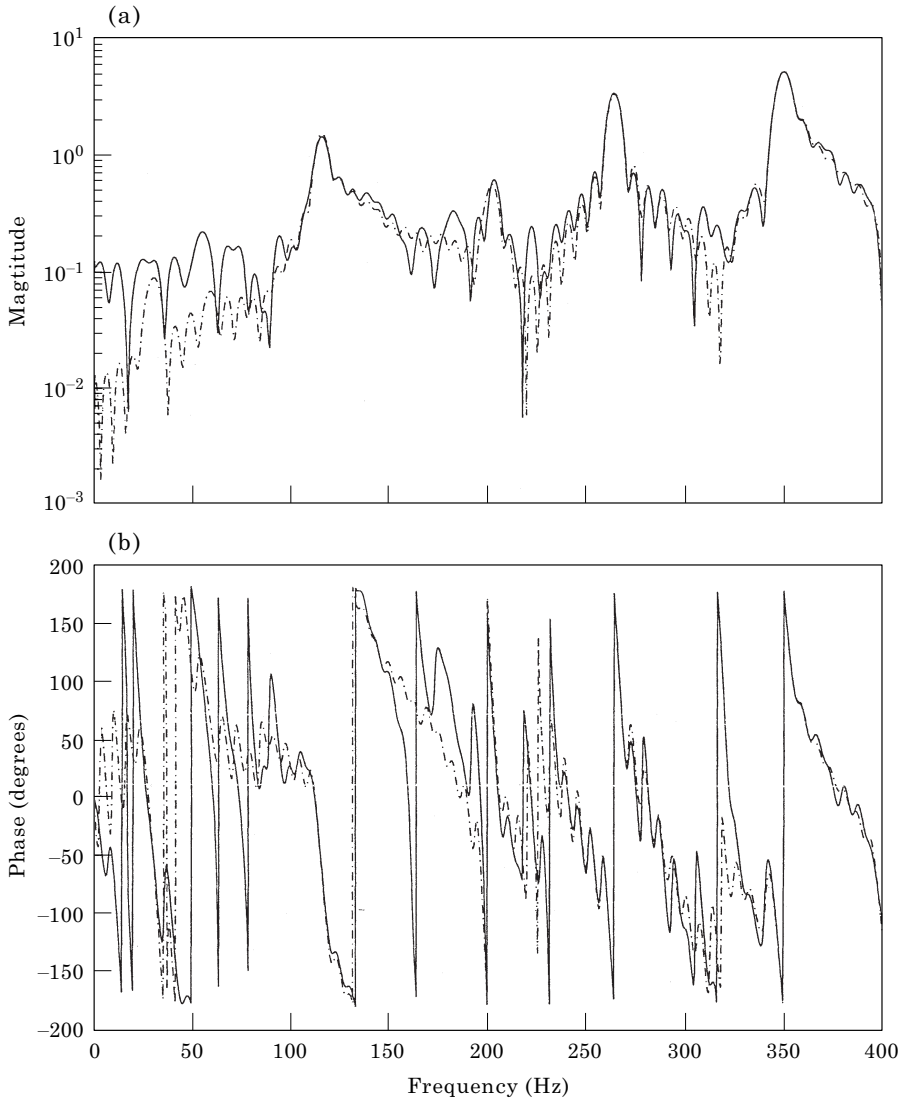

Figure 10. Frequency response functions ((a) magnitude, (b) phase) of two similar primary paths: —, primary path no. 1; –·–·–, primary path no. 2.

generator passing through a high-pass filter with the cut-off frequency at 160 Hz. Thus, each noise source occupies a different frequency range. Each of the two filters in MRMI has 128 coefficients, and the only filter in MRSI also has 128 coefficients. The power spectral density of the error signal before and after optimum control is shown in Figure 9. The result shows that the performance of both configurations is close. In fact, the overall noise reductions for MRSI and MRMI are 13·7 and 15·1 dB, respectively. The slight performance difference is due to the spectrum leakage around the cut-off frequency and different total number of filter coefficients. Theoretically, the same performance can be achieved if the reference signals occupy non-overlapped frequency range. However, since MRSI has a very simple structure, a significant amount of computations can be saved. It is interesting to note that, under the assumption that each noise source has a unique frequency range, the MRSI approach is conceptually the

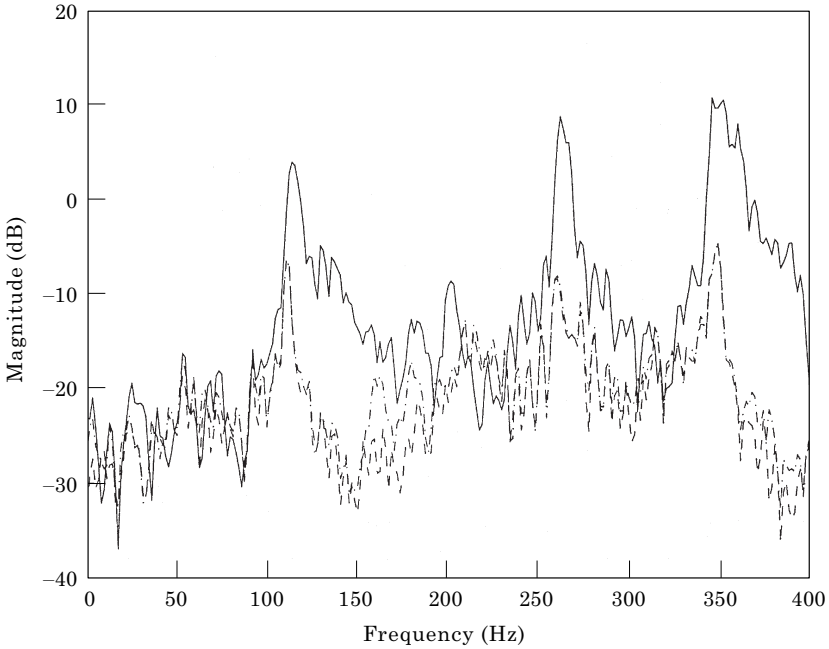

Figure 11. Spectrum of error signal when two primary paths are similar: —, before control; –·–·–, with MRSI control; – – –, with MRMI control.

inverse of the sub-band approach. In speech signal processing, in order to fully exploit the masking effect of human auditory perception, the speech signal is sometimes filtered into different frequency ranges using band-pass filters, and each frequency range is processed independently according the signal characteristics in the particular frequency range [13].

It has been theoretically predicted that if all the primary paths are similar to each other and each noise source is available as a reference signal, then MRSI is expected to have comparable performance as MRMI. In this simulation, the first primary path is replaced by the variation of the second primary path. Each coefficient of the FIR model of the second primary path is multiplied by a random number in the range of 0·75 to 1·25 to obtain a new set of coefficients, which is served as the model for the first primary path. Thus, the two primary paths are similar, as shown in Figure 10. The power spectral density of the error signal before and after optimum control is shown in Figure 11. The overall noise reductions for MRMI and MRSI are 15·3 and 14·8 dB, which clearly indicates that the performance of both configurations is very similar.

5. CONCLUSIONS

A frequency domain optimum solution of a multiple reference active noise control (MRANC) system based on a general configuration (MRMI) has been derived, and the coupling effect between noise sources and reference sensors has been considered. Another simplified control configuration in which the reference signals are directly added together to form a single signal has been investigated and compared with the MRMI configuration. When there are several noise sources, the MRMI configuration generally performs much better than the MRSI configuration. However, when each reference signal occupies a unique frequency range, or all the primary paths are similar to each

other and each noise source is available as a reference signal, the two configurations can result in comparable noise reduction. In this situation, since the MRSI configuration is much less complex, a significant amount of computational and memory saving can be achieved.

ACKNOWLEDGMENTS

The authors gratefully acknowledge the support of this work by the office of Naval Research under Grant ONR N00014-94-1-1140; Dr Kam Ng, Technical Monitor.

REFERENCES

1. C. R. Fuller and A. H. von Flotow 1995 *IEEE Control Systems December*, 9–19. Active control of sound and vibration.
2. P. A. Nelson and S. J. Elliot 1992 *Active Control of Sound*. San Diego: Academic Press.
3. T. J. Sutton, S. J. Elliott, A. M. McDonald and T. J. Saunders 1994 *Noise Control Engineering Journal* **42**, 137–147. Active control of road noise inside vehicle.
4. R. J. Alfredson 1977 *Journal of Sound and Vibration* **55**, 487–494. The partial coherence techniques for source identification on a diesel engine.
5. M. E. Wang and M. J. Crocker 1983 *Journal of the Acoustical Society of America* **74**, 861–872. On the application of coherence techniques for source identification in a multiple noise source environment.
6. D. Otte, F. Fyfe, P. Sas and J. Leuridan 1988 *International Conference on Advances in the Control and Refinement of Vehicle Noise*, *Institute of Mechanical Engineers*, *London*, *U.K.*, 123–132. Use of principal component analysis for dominant noise source identification.
7. C. M. Heatwole and R. J. Bernhard 1996 *Noise Control Engineering* **44**, 35–43. Reference transducer selection for active control of structure-borne road noise in automobile interiors.
8. S. M. Kuo and D. R. Morgan 1996 *Active Noise Control Systems: Algorithms and DSP Implementations*. New York: Wiley.
9. S. Haykin 1991 *Adaptive Filter Theory*. Englewood Cliffs, NJ: Prentice-Hall; second edition.
10. P. Z. Peebles 1987 *Probability*, *Random Variables*, *and Random Signal Principles*. New York: McGraw-Hill; second edition.
11. G. W. Stewart 1973 *Introduction to Matrix Computations*. London: Academic Press.
12. A. A. Giordano and F. M. Hsu 1985 *Least Square Estimation With Applications to Digital Signal Processing*. New York: Wiley.
13. R. Crochiere and J. Tribolet 1979 *Journal of the Acoustical Society of America* **66**, (6). Frequency domain techniques for speech coding.